Electronic Supplementary Material (ESI) for Journal of Materials Chemistry C.
This journal is © The Royal Society of Chemistry 2023

Towards persistent phosphors deliberate design: study of La-Ga admixing in LuAG:Ce crystals to engineer elemental homogeneity and carriers trap depths

Karol Bartosiewicz[1*], Verena Fritz[2], David Van der Heggen[2], Damian Szymanski[3], Justyna Zeler[4], Jan Pejchal[5], Akihiro Yamaji[6], Romana Kucerkova[5], Alena Beitlerova[5], Shunsuke Kurosawa[6,7,8,9]Akira Yoshikawa[6,7], Philippe F. Smet[2], Eugeniusz Zych[4], Martin Nikl[5]

[1]Faculty of Physics, Kazimierz Wielki University in Bydgoszcz, Powstancow Wielkopolskich 2, 85-090, Bydgoszcz, Poland
[2]LumiLab, Department of Solid State Sciences, Ghent University, Krijgslaan 281/S1, Ghent, 9000, Belgium
[3]Institute of Low Temperature and Structure Research, Polish Academy of Sciences, Okolna 2, Wrocław, 50-422, Poland
[4]University of Wrocław, Faculty of Chemistry, 14 F. Joliot-Curie Street, Wrocław 50-383, Poland
[5]Institute of Physics, Academy of Sciences of the Czech Republic, Na Slovance 1999/2, 182 00 Praha, Czechia
[6]Institute for Materials Research, Tohoku University, 2-1-1 Katahira Aoba-ku, Sendai, Miyagi 980-8577, Japan
[7]New Industry Creation Hatchery Center, Tohoku University, 2-1-1 Katahira Aoba-ku, Sendai, Miyagi 980-8577, Japan
[8]Institute of Laser Engineering, Osaka University, 2-6 Yamadaoka, Suita, Osaka 565-0871, Japan
[9]Faculty of Science, Yamagata University,1-4-12, Kojirakawa-machi, Yamagata 990-8560, Japan

* *E-mail of the corresponding author: karol@ukw.edu.pl*

SUPPLEMENTARY INFORMATION

1. Cathodoluminescence

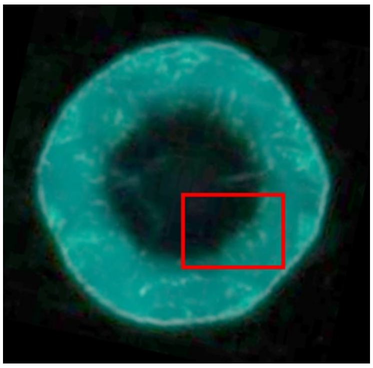

Fig. S1. The image of the non-codoped sample (La = 0.000%) with the red square indicating the area where the CL measurement was performed.

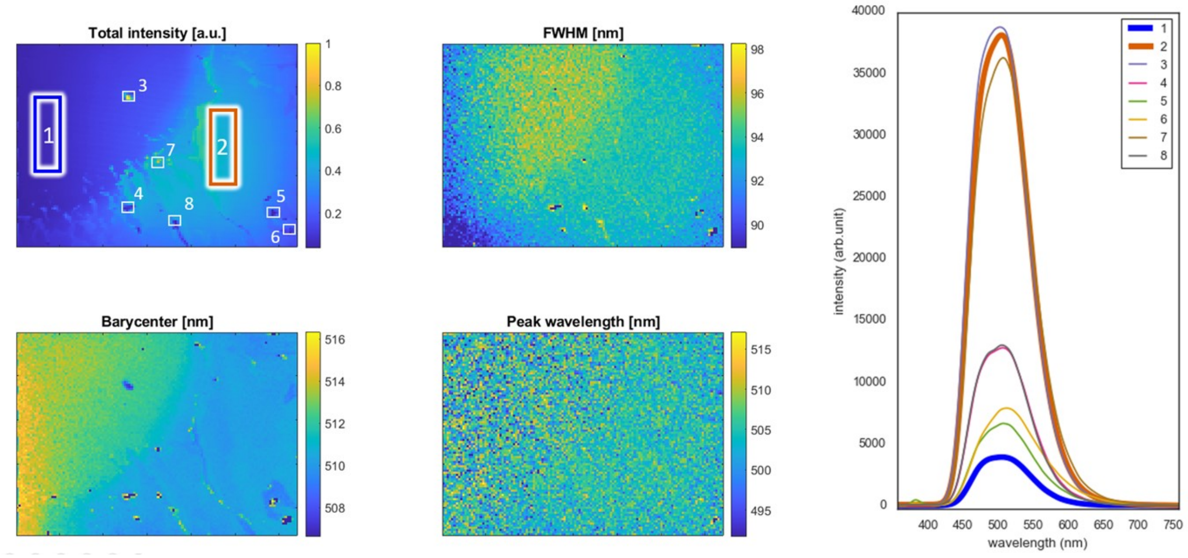

Fig. S2. Cathodoluminescence maps (of the area depicted in S1) of the total intensity, FWHM, barycenter, and peak wavelength for La = 0.000% crystal. The average spectra of the areas indicated on the total intensity map are plotted on the right side of the Figure.

Comparing the spectra (Fig. S2) of area 1 (the transparent part of the sample) and area 2 (the rim of the sample) in La = 0.000% crystal, a strong increase in intensity moving from the central part to the rim of the crystal is obvious. This observation shows that the rim of the sample is mainly responsible for the cathodoluminescence. The barycenter map and the FWHM map show that the shape of the spectra changes from the center of the sample to the rim. The decrease in luminescence intensity at the edges of the maps is caused by factors related to the apparatus and should not be discussed in this context. Nevertheless, these results proved that the rim area of the crystal shows brighter cathodoluminescence than the center of the sample. The change in the shape of the cathodoluminescence spectra assures that Ce^{3+} experiences some differences in their local environments.

2. EDS elemental mapping

Fig. S3a shows a global elemental EDS mapping of lanthanum (La). The brighter spots mainly distributed on a crystal rim reflect the higher concentration of La atoms. Fig. S3b shows a local multielemental EDS mapping of lutetium (Lu), aluminum (Al), gallium (Ga), cerium (Ce), and oxygen (O).

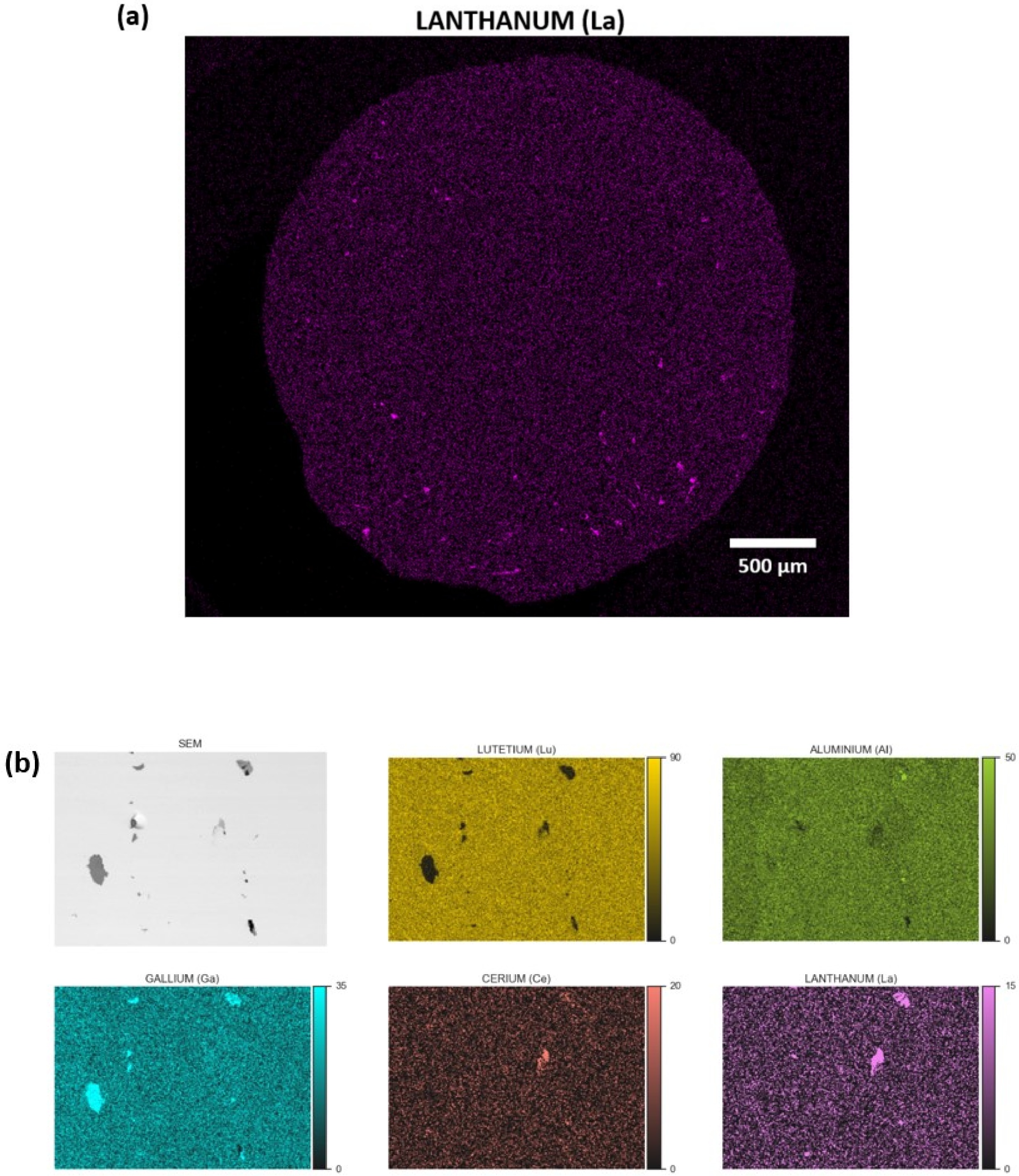

Fig. S3. (a) Global elemental EDS mapping of lanthanum (La), and (b) local multi-elemental maps of a close-up of the rim of the LuAGG:Ce0.075%,La0.300% crystal.

3. Photoluminescence characteristics

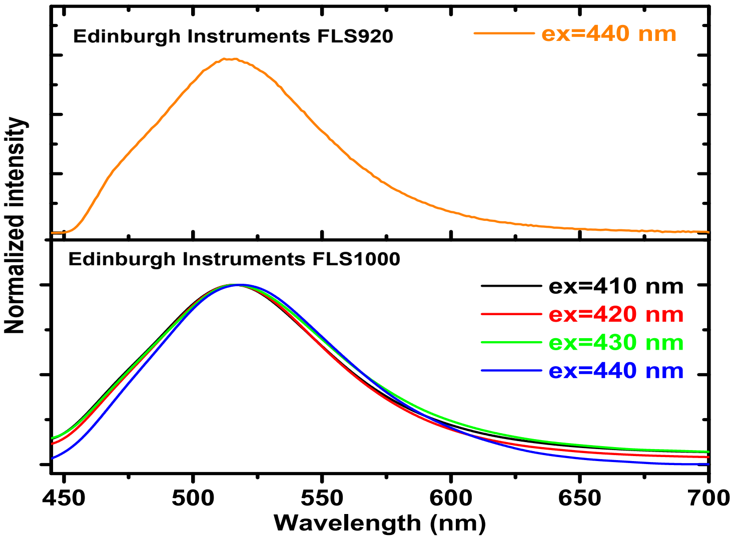

Fig. S4. Normalized photoluminescence emission spectra of LuAGG:Ce0.075%,La0.075% crystal exited at 410, 420, 430, and 440 nm. The emission spectra were recorded at Edinburgh Instruments FLS920 and Edinburgh Instruments FLS1000.

Fig. S4 compares photoluminescence spectra excited at 410, 420, 430, and 440 nm and recorded at Edinburgh Instruments FLS920 (top) and Edinburgh Instruments FLS1000 (bottom). The spectra confirm that the irregular shape of the Ce^{3+} $5d_1 \rightarrow 4f$ emission is not due to the set-up-induced distortion, but can be caused by the reabsorption process. Furthermore, the reabsorption process is well visible in Fig. 11a.

4. Temperature dependence of ns decay times

4.1 $Lu_3Al_3Ga_3O_{12}$:Ce0.075%

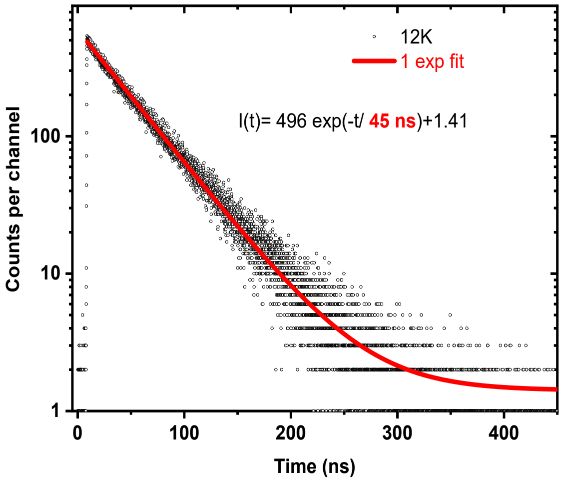

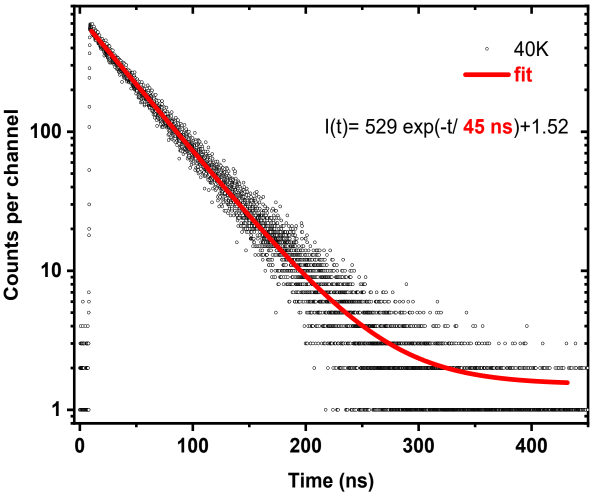

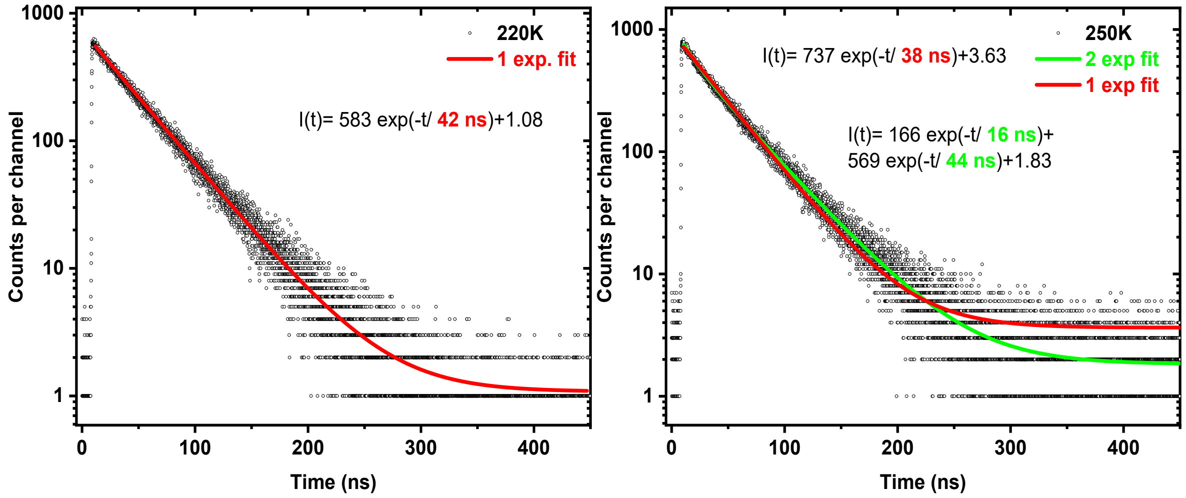

Fig. S5. Photoluminescence decay time curves of Ce^{3+} $5d_1 \rightarrow 4f$ emission at 520 nm excited at 450 nm in $Lu_3Al_2Ga_3O_{12}$:Ce0.075% recorded at 12, 40, 220, and 250 K. The solid lines represent the relevant fits.

4.2 $Lu_3Al_2Ga_3O_{12}$*:Ce0.075%,La=0.300%*

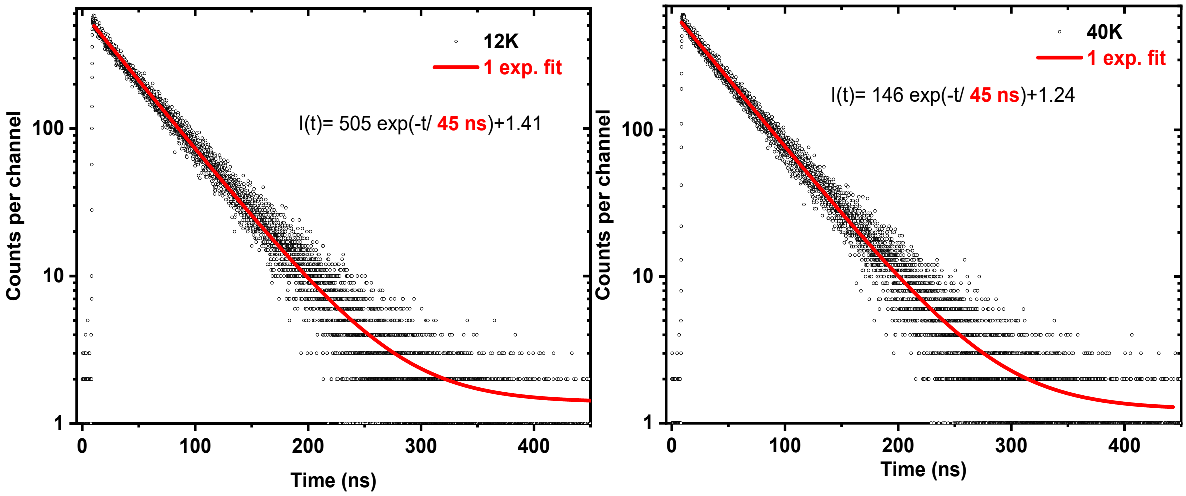

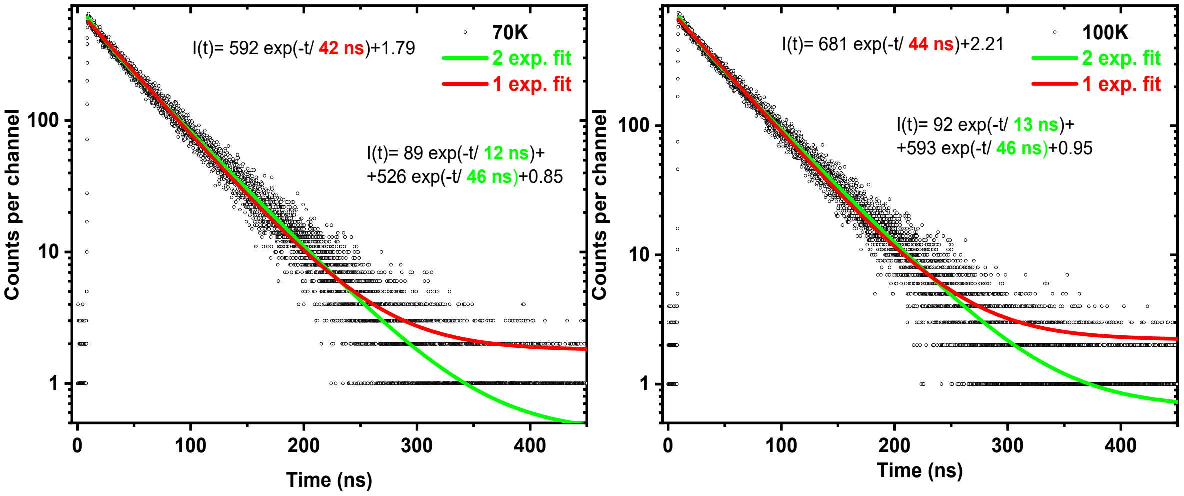

Fig. S6. Photoluminescence decay time curves of Ce^{3+} $5d_1 \rightarrow 4f$ emission at 520 nm excited at 450 nm in Lu$_3$Al$_2$Ga$_3$O$_{12}$:Ce0.075%,La0.300% recorded at 12, 40, 70, and 100 K. The solid lines represent the relevant fits.

Figs. S5 and S6 show the decay curves of Ce^{3+} luminescence in La free and La = 0.300% codoped crystals recorded between 12 and 250 K. In the La free samples, the decay curves show a single exponential character up to around 220 K. Interestingly, in the La = 0.300% codoped Lu$_3$Al$_2$Ga$_3$O$_{12}$:Ce0.075% crystal, the decay curves possess a single exponential character up to 40 K.

4.3. Single-barrier quenching model

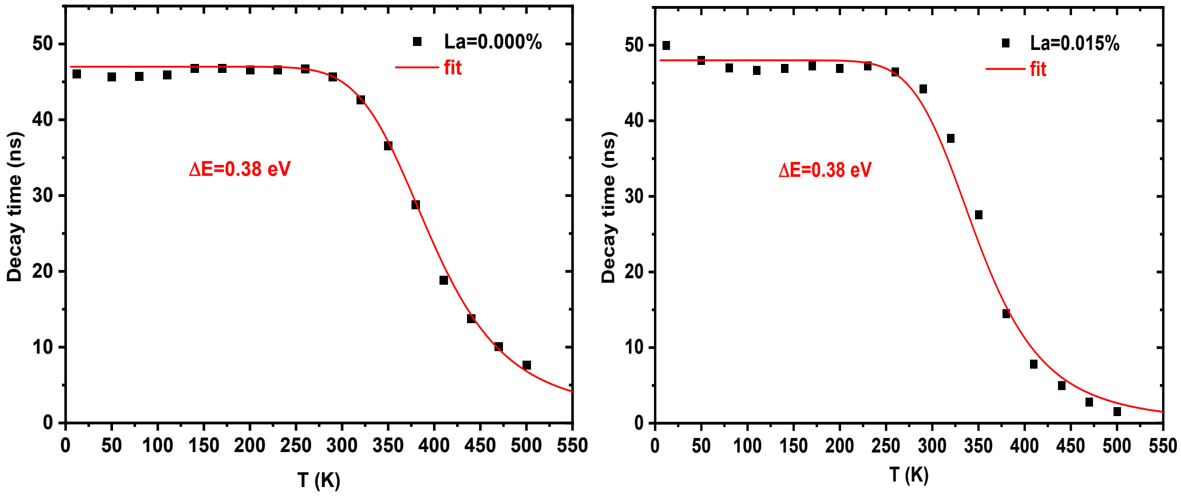

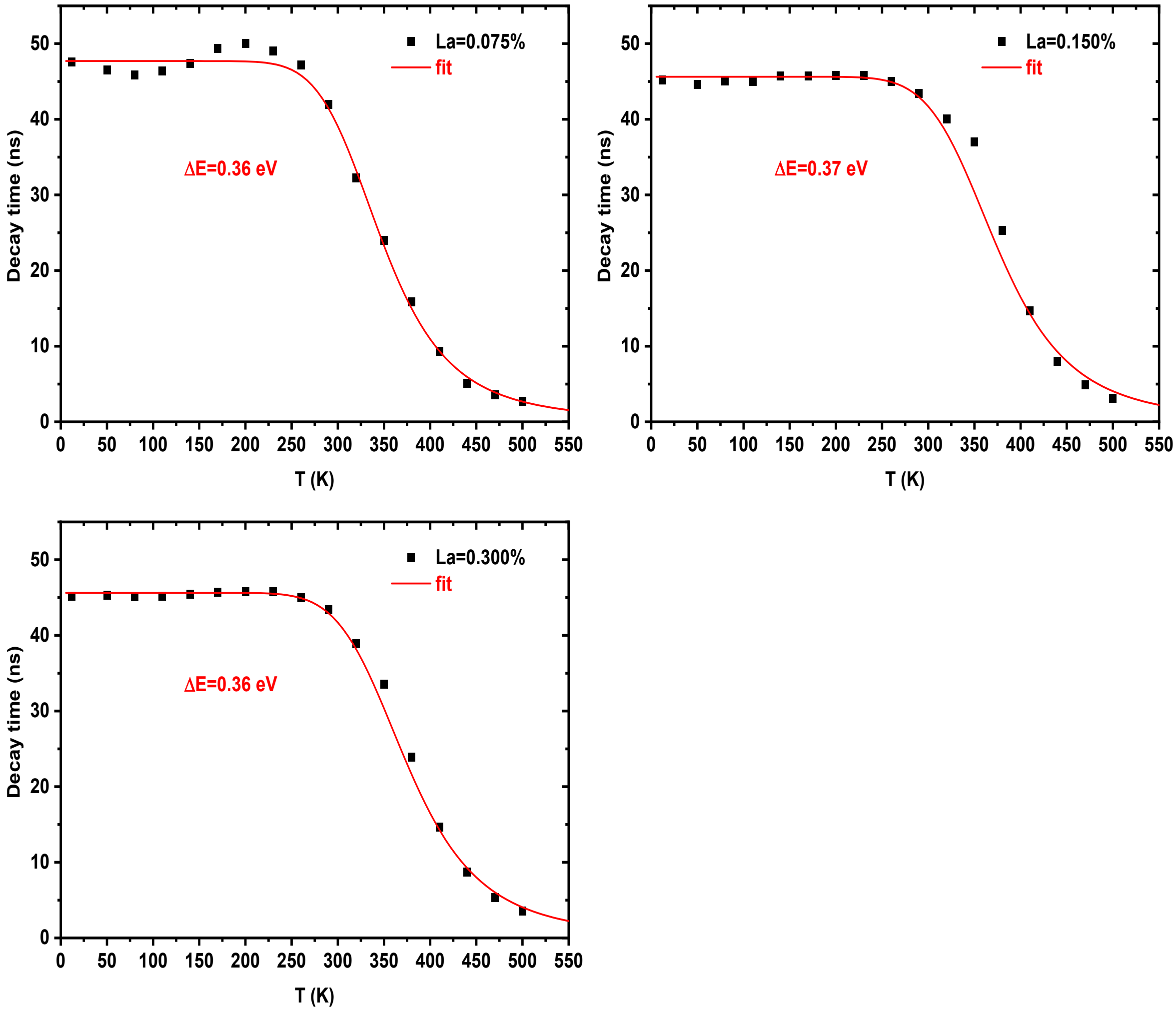

Figs. S7. Temperature dependence of decay constants for LuAGG:Ce^{3+},La^{3+} (La = 0.000, 0.015, 0.075, 0.150, and 0.300%) for excitation at 450 nm. The solid lines represent the fits of a single barrier quenching model. Note, that for the more accurate fitting of the single barrier quenching model, all decay curves were fitted with a double exponential function (Equation 1).

Figs. S7 shows the temperature dependence of the photoluminescence decay constants for LuAGG:Ce^{3+},La^{3+} with increasing concentrations of La^{3+} ions. All decay curves can be adequately described by a single-barrier quenching model (solid lines) according to Equation S1:

$$\tau(T) = \frac{1}{\Gamma_r + \Gamma_n exp(-\Delta E/k_B T)} \tag{S1}$$

where Γ_r is the radiative rate, Γ_n is the attempt rate of nonradiative processes, k_B is the Boltzmann constant and ΔE is the activation energy of the overall quenching behavior. ΔE is found to decrease from 0.38 eV for the La-free sample to 0.35 eV for the crystal with La concentration corresponding to 0.015%, (Tab. S1 and Figs. S7). Calculating the activation energy for the thermal quenching process in LuAGG:Ce^{3+},La^{3+} crystals can unravel the underlying mechanism of the luminescence quenching for Ce^{3+} ions. The magnitudes of ΔE varying between 0.35 eV and 0.38 eV suggest that thermal ionization of the $5d_1$ exited state of Ce^{3+} appears to be involved in the thermal quenching of Ce^{3+} luminescence. In general, thermal quenching by thermal ionization can be finely tuned via different cation co-substitution strategies.

Tab. S1. Compilation of the activation energy for the overall quenching behavior obtained from decay time constants.

La concentration (%)	ΔE (eV)
0.000%	0.38
0.015%	0.35
0.075%	0.36
0.150%	0.37
0.300%	0.36

4.4. Correlation between the TL and DR curves

Fig. S8 compares the thermally-induced detrapping of charges (seen by the glow curves, solid lines) and the kinetics of the $5d_1 \rightarrow 4f$ luminescence of Ce^{3+} ions, specifically, its afterglow (long) component (dots). The intensity of delayed radiative recombination (afterglow) starts to rise at a temperature higher by about 20 – 40 K than at the beginning of the TL curve. This difference is not surprising at all, as the afterglow appears when the temperature is high enough to thermally move the electron optically excited to the $5d_1$ level up to the conduction band. The TL glow curves, in turn, represent the thermally stimulated raise of the electron occupying a trap level under the conduction band. In conclusion, the trap level is closer to the conduction band than the $5d_1$ of Ce^{3+}.

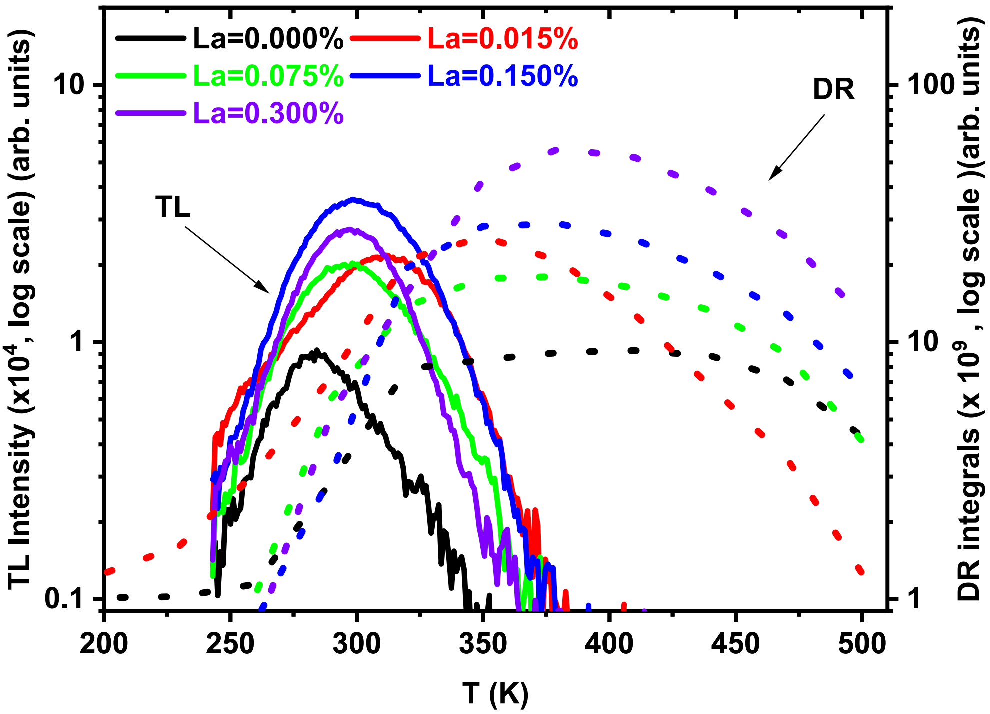

Fig. S8. Comparison of the TL (thermoluminescence) and DR (delayed radiative recombination/afterglow) curves of LuAGG:Ce crystals for crystals with different La codopant concentrations.